Shining Light On Click Adhesives!
Influence of surface modification &
crosslinker content on UV cured thiol-ene based adhesives

Bachelor's Project Thesis

Pradnesh Umesh Mahadeshwar, S4611470, p.u.mahadeshwar@student.rug.nl
Supervisors: prof. dr. R.K Bose & Yizeng Di

Abstract:

Adhesives, like social beings, hold things together- they are a crucial part of human society and are on the constant verge of development in various directions. Thus, this paper delves into one of those directions, studying the complex interplay and relationships of surface modified light induced thiol-ene click adhesives. Utilising several techniques such as FTIR, SEM imaging, lap shear tests, theoretical calculations and statistical tools, it was confirmed that the iCVD PAMA coated surfaces did significantly improve the adhesive strengths. Furthermore, the polysulphide with a higher SH content and a lower viscosity outperformed the other variant. The correlation between the adhesive strength and the quantity of crosslinkers yielded very interesting trends, diverging from the initial project hypothesis. The results obtained allowed for various theories to arise, which are discussed in detail.

Keywords: Adhesives, click reaction, thiol-ene, polysulfides, iCVD, photopolymerisation, UV curing & adhesive failures.

1 Introduction

Adhesives are everywhere around us, from holding components in our smartphones, to aiding barnacles to attach their bodies to ship hulls. The earliest evidence of adhesives used by hominins dates back to around 220,000 B.C. in modern-day Italy.[1] Stone arrowheads were glued to a shaft with tar made from the bark of a birch tree. Several other ancient civilisations also utilised adhesives which improved their technology and lifestyle. Gum Arabic from the acacia tree was a common adhesive used by ancient Egyptians in their daily life.[2]

Therefore, it is evident that humans have been using adhesives of natural origin for an extensive period for several applications, such as making rudimentary paper, tools, and constructions. In today's world, adhesives hold prominent significance beyond their traditional applications and have become more sophisticated than their predecessors.

Adhesives are synthesised to be pressure-sensitive, heat-resistant, flexible, and have several other properties. Tapes, sticky notes, and stickers are great examples of pressure-sensitive and flexible adhesives[3] These types of adhesives do not undergo a chemical reaction, making them favourable to remove and reapply elsewhere, without causing severe damage to the surface. The first adhesive tape was invented by Richard Drew in 1930[4]—after nearly a century, tapes have become a crucial part of humanity.

Tapes and various other alternatives have been integral to our daily routines, serving a multitude of purposes. It is important to note that, while this is only one type of adhesive, there are countless other adhesives with broader applications. These range from wood glue to special grade adhesives that are resistant to temperature fluctuations used in aerospace industries.[5] Adhesives are essential for societal and technological progress, influencing many areas of daily life and industrial operations.

Adhesive technology is vast, limited only by creativity. With numerous new adhesives and processes constantly emerging, it is important to research, test, and uncover their properties and mechanics.

1.1 Theory Of Adhesives

Adhesives exhibit various molecular interactions, they have interactions between themselves (cohesion) and interactions with the surface (adhesion). Together, these two forces allow for the successful bonding of two surfaces. Two types of bonding are possible—primary and secondary.[2] Primary bonding refers to chemical bonding between atoms,

known as intramolecular forces, and secondary bonding refers to intermolecular forces, commonly known as Van der Waals forces, consisting of hydrogen bonding and dipole-dipole interactions.[6]
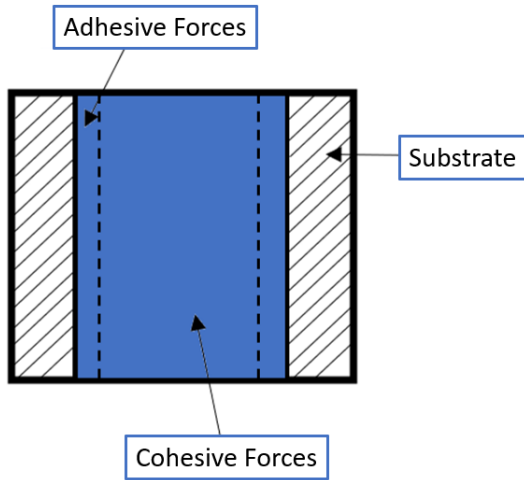
Figure 1.1: Simplistic adhesion diagram, showcasing the adhesive and cohesive forces of an adhesive between two surfaces. The dashed lines signify the boundary layers of the adhesive interface with the substrate.

Figure 1.1, illustrates a simple adhesion diagram, representing the key forces, adhesion and cohesion. The blue substance between the two surfaces is assumed to be the adhesive material. The image can be used to visually understand the previously mentioned interactions of surface-adhesive and adhesive-adhesive.

Adhesives can be primarily or secondarily bonded to surfaces. In primary bonding, the adhesive molecules undergo a chemical reaction with the surface molecules, thereby chemically bonding to the surface. The adhesives that this study focuses on are an example of primary bonding.[2]

In secondary bonding, adhesives seep into small cracks in the surface and harden. The adhesive grips the surface, and Van der Waals forces are responsible for the interactions. Adhesives like pressure-sensitive tapes serve as an example of secondary bonding.[2]

The aforementioned adhesive mechanism is for the adhesion force, for the cohesive force—the mechanism is similar. The adhesive molecules themselves can chemically react with each other, forming a network, or the adhesive molecules are physically entangled and overlap with each other such that the effects of Van der Waals forces are high.

Adhesive molecules are large macromolecules, such as natural proteins or synthetic polymers. Cyanoacrylate, commonly known as Super Glue, is a monofunctional monomer that rapidly polymerises together

in the presence of moisture on the surface to form long chains, creating a strong bond.[7] Long-chain molecules are generally preferred as they enable strong Van der Waals forces, allowing stronger interactions.

Adhesive molecules must be long; however, one can already guess a predominant disadvantage of using long-chained/high molecular weight molecules. The viscosity of such an adhesive would be too high to be applicable in real life. Therefore, adhesives are usually monomers which later polymerise, this allows the adhesive to have lower viscosity, hence good wettability to seep through the pores of the surfaces.

Additionally, other molecules such as crosslinkers or photoinitiators are also added to improve the strength and application of the adhesive. Adding crosslinkers significantly improves the cohesion between the adhesive molecules—it creates a matrix network and since it is a chemical bond between the adhesive molecules rather than Van der Waals interactions, the strength is greater.[8]

The addition of photoinitiators greatly widens the application of an adhesive. It allows spatial and temporal control of the polymerisation.[9]

1.2 Adhesion Failure

Eventually, all adhesives will undergo failure, this depends on the type of adhesives, the environment the adhesive is subjected to, the duration of time after curing, and the loading they experience. However, this study is limited to examining physical stresses. There are two main categories of physical failures, adhesive and cohesive failure. As implied by their names, adhesive and cohesive failure occur when the adhesion and cohesion forces are disrupted.[10]
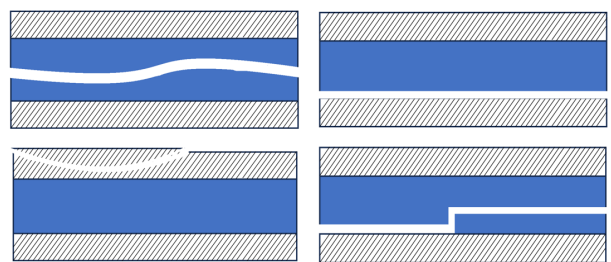
Figure 1.2: Types of adhesive failure: Cohesive failure (*Top Left*), adhesive failure (*Top Right*), adherent failure (*Bottom Left*) & combination of cohesive and adhesive failure (*Bottom Right*).

When an adhesive is subjected to a load, cracks may appear and propagate. It depends on the relative strengths of cohesion, adhesion & the adherent, to determine which type of failure will occur. If the crack propagates through the bulk of the adhesive, thereby separating the two surfaces with adhesive, it is cohesive failure—as the adhesion forces were stronger than the cohesion forces. For

an adhesion failure, the interaction between the adhesive and surface is weak, relative to the cohesive forces and when subjected to a load, bonds at the surface break, leaving one of the surfaces with no adhesive residue and the other with all the adhesive residue. Note that these are ideal failures; in reality, a mixture of the two failures is seen. Another failure is possible, adherent failure. Adherent failure occurs when the adhesive is much stronger than the adherent, or surface. Here, the opposite happens; the adhesive is undamaged and the surfaces are broken. Refer to *Figure 1.2* for a visualisation of these failures.

Let us put these types of failures into a familiar scenario. Think about opening an Oreo cookie—if all the cream sticks to one half, that is adhesive failure. If both halves retain the cream, that is cohesive failure. A combination of these two failures would result in an uneven distribution of cream, with some areas having cream and some none. If either of the halves of the Oreo break upon opening, and the cream remains intact, that is adherent failure.

To prevent the previously mentioned failures, various techniques/processes can be applied to the adhesive and substrates. This study specifically aims to avoid adhesive failure by enhancing the interaction between the substrate and the adhesive bulk. To mitigate such a failure, surface modification techniques can be carried out—one particular technique is iCVD.

1.3 Initiated Chemical Vapor Deposition (iCVD)

Surface modifications are a powerful tool in material science. They allow the surface of a material to enhance the physical, chemical and mechanical properties without altering the bulk properties of the materials. Coatings may be applied to surfaces to make them resistant to corrosion or water (hydrophobic). After surface modification, the surface energy and thus the wettability of a material changes. Hence, it is easier for the materials to maintain their original bulk properties while being used in various environments.[11]

Multiple surface modifications are available, such as plasma treatment, coating, or surface functionalisation. In this study, surface modification is achieved by applying a polymer coating via iCVD technique. iCVD stands for initiated chemical vapour deposition. Conventional surface modifications can often cause damage, such as swelling, to the material, as they involve the use of solvents. However, iCVD overcomes these limitations with the use of solvent-free polymerisation, also making it a green process.

In a vacuum chamber, volatile monomer and initiator are introduced simultaneously in vapour form. These vapours pass through an array of heated filaments, causing the thermal conversion of the initiator to reactive radical species. The reactive radical species and monomer are absorbed upon reaching the cooled stage, and undergo free-radical polymerisation. The iCVD method therefore only requires monomers and initiators, no solvents are required and no further purification steps are needed. It can preserve the coating's functionality without harming the surface, making them suitable for biological and electronic applications,[12], [13] and is also one of the main reasons why this technique was chosen for the study.

It is possible to take advantage of iCVD's ability to preserve the functionality of the coating without harming the substrate, to enhance the interaction between the adhesive bulk and the surface of the substrate. This can be done by coating the substrate with functional group A and using an adhesive with functional group B, and under some condition, the two functional groups can react to form a bond A-B. These new primary bonds would reduce the chances of adhesion failures and increase adhesive strengths. Thiol and ene were the two functional groups that were used during this study.

1.4 Thiol-Ene Click Chemistry

Sharpless et al. termed "click" chemistry in 2001.[14] The term "click" is derived from the analogy of buckling on a seat belt. For a reaction to be categorised as a click reaction, it has to follow strict criteria.[15] For example, the process should utilise no solvent or a benign solvent, and generate none or inoffensive byproducts that can be easily removed via nonchromatographic methods.

Thiol-ene reactions are deemed to be click reactions. Two different mechanisms are possible for the reaction to proceed through: free-radical addition and catalyzed Michael addition. This research project will solely focus on free-radical addition initiated via light, a specific area within photochemistry.[16]

Thiol-ene reaction is a reaction between a thiol compound and an ene compound, a carbon-carbon double bond, forming a thioether molecule. Refer to *Figure 1.3*.

$$R-SH + R' \overset{\text{Driving Force}}{\longrightarrow} R^{\diagdown S \diagdown \diagup} R'$$

Figure 1.3: Thiol-ene reaction forming a thioether, here the driving force can be heat, a catalyst or light irradiation.

Due to the solvent-free and low temperature reaction conditions, the light initiated thiol-ene reaction is compatible with the iCVD technique. Thus, the thiol and ene functional groups were chosen for the adhesive and coating respectively.

1.5 Photochemistry

Photochemistry is a branch of chemistry consisting of chemical reactions initiated or influenced by light. Electronically excited molecules are responsible for these photochemical reactions. These excited molecules are generated via absorption of light in the visible and near UV regions. This project will not delve deep into the theory of photochemistry—if the reader is curious, please refer to N.J. Turro et al.[17] "Principles Of Molecular Photochemistry, An Introduction."

This thesis will focus on a niche set of adhesives that cure via UV radiation. In the 1960s, UV light was used in the curing process for fixing varnishes on furniture; this technique was commercialised in the following decade.[18]

UV radiation is known to be harmful to plastics, in the case of prolonged exposure to direct sunlight. UV radiation breaks down the bonds in plastics, degrading them, and causing significant changes in their optical and mechanical properties.[19] These are typically seen as yellowing and brittleness, respectively. Nevertheless, as previously mentioned, it is beneficial because it rapidly initiates polymerisation.[20]

The main advantages of UV curing are the spatial and temporal control over the polymerisation.[21] Selective regions of a medium can be polymerised, which has led to the invention of 3D printing with UV. The temporal advantage allows mixing of components for polymerisation and then curing them later by exposing them to UV light. Additionally, curing can be done without solvents, and even from a distance, making it ideal for applications such as semiconductor fabrication[22] and hardening composite veneers in dental patients.[23]

1.5.1 Photo-polymerisation

Photo-polymerisation is a niche part of photochemistry that is studied in this report. The general photoinitiated polymerisation for thiol-ene reaction involves the following:
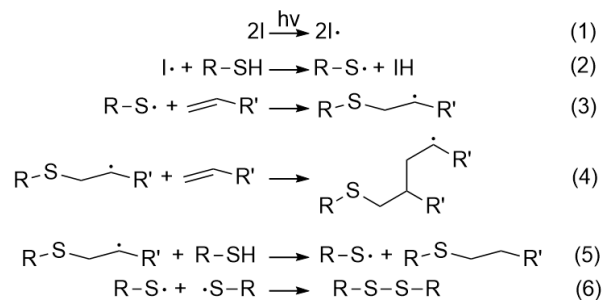
Figure 1.4: Thiol-ene polymerisation steps initiated through homolytic cleavage of photoinitiator I.

Radical formation can occur through two distinct pathways: homolytic cleavage or hydrogen atom abstraction from a donor. *Figure 1.4*, illustrates the homolytic cleavage of the photoinitiator I, into its corresponding radical after irradiation, shown in *step 1* of the process. *Step 2*, represents the monomer initiation, thiyl radical is formed from the thiol via the hydrogen abstraction by the radical initiator. The thiyl radical propagates the ene molecules via addition, shown in *steps 3 & 4*.

Step 5 demonstrates the chain transfer process, where a new thiol monomer is activated and the previously growing chain has stopped. Finally, *step 6*, shows one of many termination steps that could occur for this example, during termination, all the radicals eliminate each other by forming bonds together, thereby gradually ending the polymerisation. An alternative termination mechanism is disproportionation, in this case, one radical molecule abstracts a hydrogen atom from another radical molecule, resulting in one saturated molecule and the other unsaturated molecule.[24], [25]

There are two types of polymerisation, step-growth and chain-growth. During step-growth polymerisation, bifunctional or multifunctional monomers react together to form dimers, which then react with other similar monomers to form trimers, and so forth, eventually forming oligomers, which then form polymers. As the reaction progresses, a byproduct, typically a small molecule such as water, is released. Many active chains grow simultaneously during step growth, creating a wider range of chain lengths because of the multiple reaction pathways available. Thus, the polydispersity is greater than 1. An example of step-growth polymerisation is the formation of Nylon-6.[26], [27]

In chain-growth polymerisation, only a few active sites are available. Monomers add to a growing chain one at a time to these active sites, without producing byproducts. This process results in a narrow distribution of chain lengths, giving rise to a polydispersity of approximately 1, as monomers are sequentially added to a limited number of active sites. An example of chain growth polymerisation is the formation of polystyrene. *Figure 1.4*, represents such a chain growth polymerisation.[28]

However, these definitions of polymerisations are not concrete, confusion is also present in the field, as described by Chan et al., 2022.[28] During this research, multifunctional thiol-ene polymerisation initiated via irradiation appear to be a combination of step-growth and chain-growth polymerisation. This process is commonly defined as step-growth; however, certain characteristics of chain-growth polymerisation are present, such as no byproducts produced during the polymerisation. The types of polysulphides, photoinitiators, and crosslinkers utilised during this study are described in the following sections.

1.6 Liquid G Polysulfides

Thioplast® G polysulfide by Nouryon[29] is widely used as a sealant, typically in aerospace & construction industries, because of their outstanding properties such as: solvent resistance, low temperature flexibility, impermeable to many gases & moisture, high viscosity, and great adhesion. The main downside is the pungent smell.

Conventionally, the curing process of G polysulfides requires elevated temperatures, solvent, curing agents with strong oxidation properties (such as manganese (IV) oxide), and a relatively long curing duration.[29] These characteristics make the curing process less environmentally friendly compared to the curing method explored in this study.
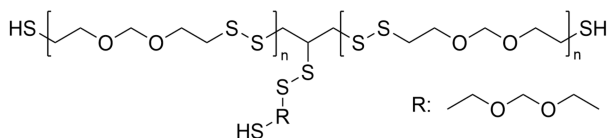
Figure 1.5: General Thioplast® G polysulfide structure.[29]

The above *Figure 1.5*, illustrates the general structure of the polysulfide.

Table 1.1: G1 & G21 polysulfide properties.[29]

Properties	Unit	G1	G21
Viscosity at 25°C	Pa s	41 - 52	10 - 15
Repeating units (n)		26 - 28	13 - 15
Specific weight	g/cm^3	1.28	1.28
Branching	%	2.0	2.0
SH - content ($x_{SH\%}$)	%	1.8 - 2.0	2.7 - 3.1

1.7 Click Adhesive Components

In this study, polysulfides G1 & G21 (*Figure 1.5*, *Table 1.1*) were used with 1,3,5-Triallyl-1,3,5-triazine-2,4,6(1H,3H,5H)-trione (TTT) as crosslinker, and 2,2-Dimethoxy-2-phenylacetophenone as photoinitiator, to produce "click adhesion" between two surfaces. Refer to *Figure 1.6*. Both the crosslinker and photoinitiator are typical chemicals used in such adhesives.
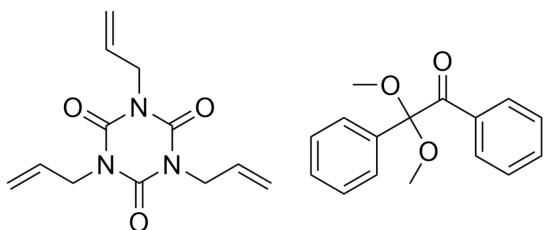
Figure 1.6: Crosslinker (*Left*) & photoinitiator (*Right*).

Surfaces were modified via a thin coating of poly(allyl methacrylate) (PAMA), which was synthesised from allyl methacrylate (AMA), as the monomer, in the presence of a thermal initiator, di-tert-butyl peroxide, The process was conducted via iCVD, see *Figure 1.7* for the schematic.
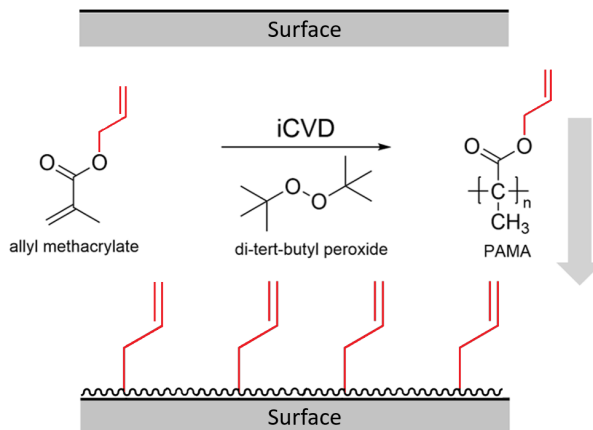
Figure 1.7: Schematic of process for iCVD coating of PAMA.
Image credit: Sung Gap Im et al.[30]

Figure 1.7, illustrates the polymerised structure of allyl methacrylate. Addition polymerisation occurs at the double bond in the acryloyl group, the chain extends through the acryloyl part of the molecule. The allyl part of the molecule is partially preserved. Thus, this creates a surface with a thin coating of PAMA, with allyl groups facing away from the surface, allowing the thiol groups from G1 or G21 to react with the coating. For better visualisation of *Figure 1.7*, only the allyl group is shown.

It is important to note that for the mentioned polymers, the reaction mechanism is very similar to *Figure 1.4*. The main difference in polymerisation is that the polysulphides and the crosslinker possess multiple thiol and ene reaction locations. Hence, multiple chains grow simultaneously from all functional sides, giving rise to a network. Additionally, as mentioned previously, the polymerisation between the polysulphide and TTT is considered to be a step-growth polymerisation, due to the multiple functional groups present on a molecule. However, there are characteristics of chain growth present as well, as no small molecule was eliminated during the reaction.

This study aims to understand *the extent to which surface modification via initiated vapour chemical deposition (iCVD) and the crosslinker content influence the strength of thiol-ene adhesives.* This was achieved by conducting lap shear tests on adhesives of different crosslinker content, without and with iCVD coated surfaces. Three different surface materials were utilised: glass, polycarbonate, and aluminium. The polymerisation was confirmed and characterised with FTIR. The final results

were statistically analysed via ANOVA with a post-hoc Tukey HSD. Theoretical calculations on the efficiency of the coating were also utilised.

Hypothesis:

Increasing crosslinker content in the adhesive, will increase the adhesive strength until an optimum point, after which the correlation will be negative, as adding more crosslinker results in a stronger network forming, improving the cohesion. However, increasing crosslinker amount, will lead to the adhesive becoming hard and brittle, causing cracks to propagate easier, and thereby lowering the adhesive strength.

iCVD coating, will significantly improve the adhesive strength, as the adhesion forces would be much stronger than for non-coated samples, due to the interlocking of the surface with the bulk of the adhesion, and to the opposite surface, ensuring a strong adhesive strength. In terms of crosslinker amount, adding a lower crosslinker amount would result in higher strength, as more SH functional groups would be free to react with the allyl groups on the surfaces. Glass & aluminium should show stronger adhesive strength than polycarbonate, as glass and aluminium surfaces were rougher than polycarbonate, hence polycarbonate having a lower surface area. Therefore, less allyl groups could be present on polycarbonate, leading to a lower adhesive strength than aluminium and glass.

2 Experimental

This section aims to guide the reader through the process of producing UV-curable thiol-ene adhesives from scratch. The iCVD process was not conducted by the author personally due to time and resource restrictions, however, a brief but informative procedure is provided. The rest of the process was conducted by the author and is explained in great detail.

2.1 iCVD Of PAMA

The PAMA coating was obtained on a cooled stage (5°C) in a vacuum chamber operating at 500 mTorr, the pressure was maintained using a capacitance manometer (MKS Instruments, Inc.) that worked in conjunction with the MKS pressure controller to manage the butterfly valve. Allyl methacrylate and di-tert-butyl peroxide were introduced in a vapour phase at flow rates of 1.4 and 0.6 sccm* respectively. The mass flow rate was controlled via a Swagelok metering valve. The polymerisation was initiated with the resistively heated stainless steel filament at 170°C. Flim thicknesses of approximately 500nm of the PAMA were obtained in 45 min. The film thicknesses were monitored *in situ* by interferometry. The iCVD machine utilised during this study was built in-house.

---

*Standard cubic centimetres per minute

2.2 Fabrication Of Adhesive

For each thioplast G21 & G1, five different adhesives were made according to varying crosslinker (TTT) contents of 1:1, 10 wt%, 30 wt%, 50 wt% & 100 wt%. To each adhesive, 1 wt% of photoinitiator was added. The weight percentages of the crosslinker were determined using *Equation 2.1*, excluding the mass of the photoinitiator as it is considered to be negligible.

$$w_{\text{TTT}}\% = \frac{m_{\text{TTT}}}{m_{\text{TTT}} + m_{\text{G21/G1}}} \qquad (2.1)$$

To determine the 1:1 molar ratio of thioplast and crosslinker, the moles of SH groups need to be equivalent to those of ene groups in the crosslinker. *Equation 2.2*, is used to calculate the moles of SH groups in the thioplast, it is the mass of the thioplast G21 or G1 divided by the molar mass of the SH group which is 33 g/mol. This value is then multiplied by the $x_{\text{SH}\%}$ SH-content of the corresponding thioplast, the SH-content can be referred from *Table 1.1*. Therefore, the moles of the SH group in the respective polysulphides can be determined.

$$n(\text{SH}) = \frac{m_{\text{G21/G1}}}{M_{\text{SH}}} \cdot x_{\text{SH}\%} \qquad (2.2)$$

Since the reaction taking place is a click reaction between a thiol and an ene, refer to *Figure 1.3*, one thiol group only reacts with another ene group. Additionally, the crosslinker molecule TTT, has 3 ene groups, therefore, to calculate the moles of TTT, the moles of SH need to be divided by 3. Refer to *Equation 2.3*.

$$n(\text{TTT}) = \frac{n(\text{SH})}{3} \qquad (2.3)$$

Finally, the mass of the crosslinker can be calculated by multiplying its molar mass, 249.27 g/mol.

$$m_{\text{TTT}} = n(\text{TTT}) \cdot M_{\text{TTT}} \qquad (2.4)$$

Table 2.1 contains the previously mentioned calculations for the respective amounts of polysulphides. It is important to note that only the molar 1:1 is segregated into G21 and G1, weight percentage values are the same for G21 and G1. The mass of the polysulphide was determined by the limited availability of crosslinker, and ensuring there was enough adhesive to stir. 5 - 3g of thioplast was deemed to be enough.

20mL glass vials were covered with aluminium foil and labelled according to the type of polysulphide and the crosslinker content. The photoinitiator, TTT, and polysulphide were sequentially added to these glass vials in that specific order. The order is essential to ensure that the photoinitiator and TTT mix well with the polysulphide. The TTT had to be preheated at approximately 50°C to liquefy it, simplifying the measuring and mixing processes.

TTT Content	TTT (g)	Thioplast (g)	Photoinitiator (g)
1:1 (G21)	0.340	5.00	0.053
1:1 (G1)	0.227	5.00	0.052
10 wt%	0.556	5.00	0.056
30 wt%	2.143	5.00	0.071
50 wt%	3.00	3.00	0.06
100 wt%	3.00	0.00	0.03

After adding all the components, the adhesives were mixed using a vortex mixer, then heated to 70 °C and stirred for approximately 3 hrs. Periodically, the adhesives were inspected to ensure homogenous mixing. Once thoroughly mixed, the adhesives were left in a fridge overnight.

2.3 Lap Shear Sample Preparation
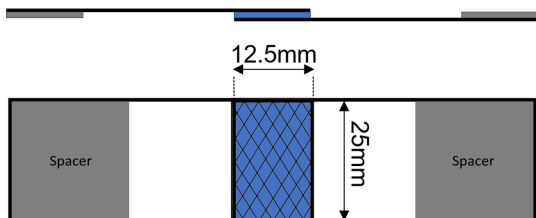
Figure 2.1: Configuration of standard lap shear area for sample. *Not to scale.*

Glass/Aluminium/Polycarbonate slides were prepared according to the dimensions shown in *Figure 2.1*. The standardised bonding area for a lap shear test is 312.5 mm^2. [31] Each sample was labelled according to the adhesive applied. The adhesive was used on one of the surfaces, and small dots of adhesives were placed at the corners and the centre via a pipette, and pressed gently but firmly with the other surface keeping in mind the area to be covered. Any air bubbles were removed with firm pressure. Once applied, the two surfaces were clamped on either side. Spacers of dimensions 25x25 mm were glued with commercial super glue to the ends to maintain equal thickness on both sides of the sample, ensuring it stayed straight when placed in the lap shear machine.

A UV lamp† was secured and samples were irradiated to cure, approximately 1.15 W/cm^2 of energy was absorbed by the adhesive. Each sample was irradiated for 3 minutes, 1 minute on each face, and 30 seconds on each edge. This made certain that all the adhesives had a chance to cure. After curing, the samples were placed in a fridge overnight. This process was repeated for PAMA-coated glass slides, aluminium (coated & uncoated), and polycarbonate

---

†Please be aware of the dangers of working with UV radiation; it is recommended to wear appropriate gloves and UV glasses.

(coated & uncoated). For each adhesive-crosslinker content, 5 samples were prepared to guarantee statistical significance during the data analysis process.

2.4 Lap Shear Strength Test

Shimadzu AGX-V tensile tester was used to test the samples. The lap shear test speed was set to 1.3mm/min until break. A pressure of 4-5 psi was considered sufficient for the pneumatic clamps. After the test, pictures of the failed adhesives were taken, to visually analyse the type of failure that occurred.

2.5 FT-IR

Shimadzu IRSpirit-T was used to conduct the FT-IR tests, the number of scans and the resolution were set to 64 and 4 respectively for all scans. Before measuring the samples, a background spectrum of the ambient surroundings was taken to ensure that the software could subtract this background from subsequent scans. The FT-IR of the adhesive before and after curing was taken. An adhesive drop was placed on the ATR crystal, and an IR measurement was taken, it was then irradiated with UV light for 3 minutes and another IR measurement was taken.

2.6 Rheology

A temperature sweep was conducted with Discovery HR-2. A temperature range from 40 - 70°C was chosen, and the adhesive was placed on a 25mm stainless steel parallel plate under atmospheric pressure inside the chamber.

3 Results & Discussion

This section will methodically examine the data obtained from FTIR, lap shear tests & sample images. Firstly, the polymerisation of the coating and the adhesives are confirmed with FTIR analysis and an SEM image. Secondly, the stress-strain curves are achieved from the lap shear tests, and these curves are examined for characteristics trends and patterns. Finally, the adhesive strength data are statistically analysed via ANOA with a post-hoc Tukey HSD.

3.1 Coating Polymerisation

An SEM image was taken of a PAMA coated silicon wafer, see *Figure 3.1*. The layers observed from top to bottom are the PAMA coating, the silicon oxide layer of the wafer, and the silicon wafer itself. However, the SEM image alone is insufficient to confirm that the coating was polymerised on the surface.

To confirm the polymerisation on the surface, FTIR measurements were taken of the AMA coated silicon wafer and iCVD PAMA coated silicon wafer, see *Figure 3.2*.
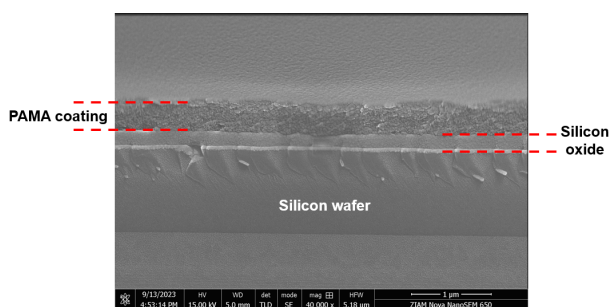
Figure 3.1: SEM image of PAMA coated silicon wafer, different layers are indicated.
Image credit: Yizeng Di
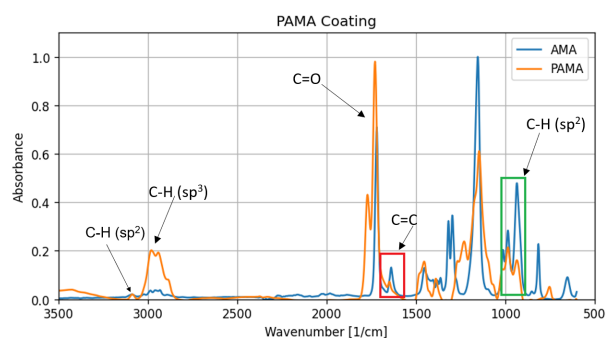
Figure 3.2: FTIR plot of AMA & iCVD coated PAMA on silicon wafer.
Data credit: Yizeng Di

The FTIR plot above indicates two curves blue and orange which are AMA and PAMA respectively. The main functional group to be observed is the C=C. The C=C bond appears in two locations within the AMA monomer: at the methacrylate vinyl and allyl positions, refer to *Figure 1.7*.

After polymerisation, the vinyl C=C bond opens up and connects to other AMA molecules, resulting in the polymerisation. The red rectangle indicates the region of 1680 - 1640 cm^{-1}, here C=C stretch at 1648 cm^{-1} shifts to 1638 cm^{-1} and reduces in intensity. The shift and reduction in intensity of the peak indicates polymerisation, proving a thorough reaction of the vinyl bonds.

The allyl -C=CH$_2$ remains partially intact after polymerisation. The green rectangle indicates the region of 986 - 935 cm^{-1}, the peaks in this region are due to the bending of the C-H (sp^2) bond, which persist after polymerisation, indicating a large retention of the pendent allyl groups. Moreover, a small peak is observed at 3091 cm^{-1}, this is due to the C-H (sp^2) stretch. Hence, it is confirmed that it is indeed the vinyl methacrylate C=C bonds that are taking part in the polymerisation, and the allyl C=C bonds are partially preserved.

Therefore, the SEM image and FTIR analyses confirmed successful polymerisation and functional group preservation on the coated surfaces.

In addition, several other peaks can also be analysed. The broad peak at 3000 cm^{-1} is due to the C-H (sp^3) stretch. The increase in the intensity of this peak in PAMA is due to the addition of the thermal initiator during the iCVD polymerisation. The initiator, di-tert butyl peroxide, has several C-H (sp^3) bonds, refer to *Figure 1.7*. The tert butyl peroxide radical can combine with another active radical on a growing chain or it can abstract a hydrogen atom and form tert butyl alcohol. *Figure 1.4* represents similar radical reactions and explanation.

The sharp peak around 1730 cm^{-1} is due to the acrylate C=O stretch. The peak is present in both AMA & PAMA, this agrees with the reaction, since polymerisation occurs only at the vinyl C=C, and hence the C=O is intact. Due to the fact that this peak is present in both and has similar intensity and wavenumber, it was used as a reference for the baseline correction.

3.2   Adhesive Polymerisation
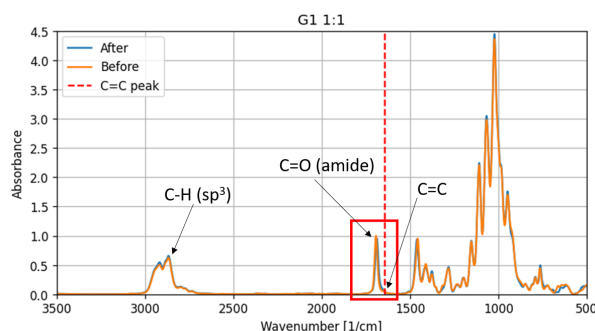
Figure 3.3: FTIR plot of G1 1:1 adhesive before (orange) and after (blue) curing. The red dashed line indicates the C=C peak.

The above FTIR plot shows the G1 1:1 adhesive before and after curing. The red dashed line indicates the TTT C=C stretch at 1645 cm^{-1}. A medium broad peak is present in the region of 3000 - 2700 cm^{-1}. This is due to the C-H (sp^3) from the G1 polysulphide, refer to *Figure 1.5*. The sharp peak at 1693 cm^{-1} is due to the amide C=O stretch, present in crosslinker TTT, refer to *Figure 1.6*. Both the C=O and C-H (sp^3) bands show no change in intensity, confirming no reactions involving these functional groups.

Whereas, the C=C peak due to the allyl functional groups present in the TTT, reduces in intensity. Refer to *Figure 3.4*, this plot shows the region between 1740 - 1600 cm^{-1}. The C=C peak is more clearly visible here, and the observed reduction in intensity confirms that a thiol-ene reaction is occurring, see *Figure 1.3*. This is similarly seen for G21 1:1, refer to *Figures B.1 & B.2*.

To confirm that the reaction is solely occurring between the C=C of TTT and the SH of the poly-
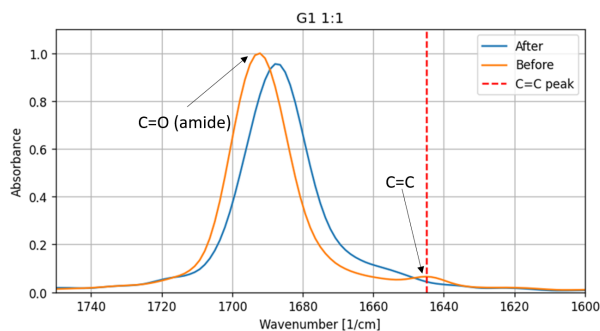
Figure 3.4: Zoomed FTIR plot of G21 1:1 in the 1740 - 1600 cm⁻¹ region.
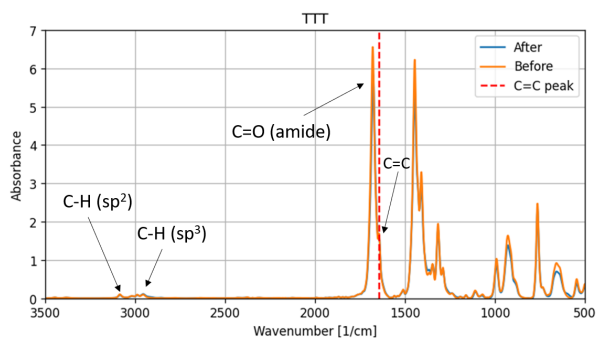
Figure 3.5: FTIR plot of TTT (100 wt%) adhesive before (orange) and after (blue) curing. The red dashed line indicates the C=C peak.

sulphides, an FTIR of TTT, 100 wt% adhesive was analysed, see *Figure 3.5*. In this plot, the intensity of the C-H (sp^3) peak is minimal because TTT contains a few C-H (sp^3) bonds. The C-H (sp^2) peaks are also visible, these are because of the allyl groups present. In G1 and G21 1:1, the C-H (sp^2) are hardly visible because the polysulphide is present in higher quantities than the crosslinker. An FTIR of G1/G21 50 wt% would likely show the C-H (sp^2) peaks of TTT.

Similarly, the C=O amide peak at 1693 cm⁻¹ and the C=C peak at 1645 cm⁻¹ show higher intensity compared to the G1/G21 1:1 plots because those adhesives contain less TTT.
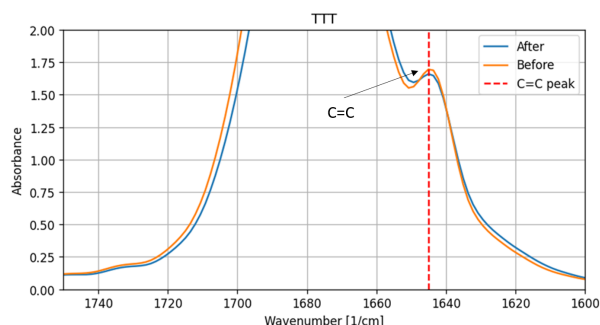
Figure 3.6: Zoomed FTIR plot of TTT (100 wt%) in the 1740 - 1600 cm⁻¹ region.

In *Figure 3.6* the C=C allyl peak of TTT is more visible, and it is clear that the intensity of the C=C peak remains unchanged. The FTIR plots before and after polymerisation appear almost identical. Therefore, the unchanged intensity of all the mentioned peaks after polymerisation confirms that TTT does not polymerise with itself, and thus polysulphides are also required.

Hence, it can be concluded that the reaction is occurring exclusively between the polysulphide and the TTT, based on the analysis of the G1 1:1 and TTT (100 wt%) FTIR spectra. However, other bonds such as S-S bonds, may be forming. However, FTIR spectroscopy is unable to detect the vibrations of thiol groups, and a different spectroscopic technique, such as Raman spectroscopy could be used to reveal new information.

3.3 Stress - Strain Curves

While FTIR spectra offered insights into chemical reactions of the polymerisation, it did not provide information about the adhesive's response to physical stress. Therefore, lap shear tests were conducted. The resulting stress-strain curves were plotted and analysed.
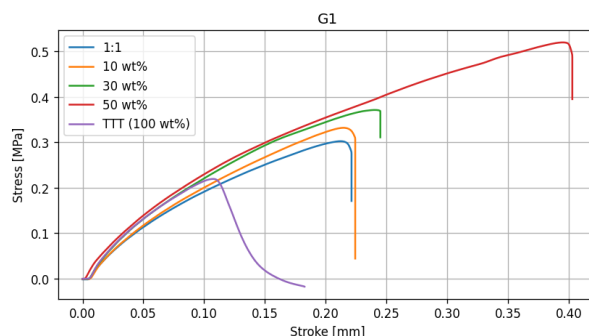
Figure 3.7: Stress - strain curve of G1 for different crosslinker amounts on uncoated glass surfaces.

Figure 3.7, represents the stress-strain curve of G1 uncoated for the various crosslinker amounts. G1 uncoated refers to the substrate not being PAMA coated. At first glance, it is evident that the TTT (100 wt%) curve (purple) exhibits the lowest maximum stress before adhesive failure. This observation aligns with the prior FTIR analysis indicating that TTT does not polymerise. Consequently, the adhesive strength, represented by the maximum stress, is lower compared to other crosslinker contents. Similarly, stress-strain curve is seen for G21 uncoated samples, refer to *Figure B.3*.

The G1 uncoated adhesive samples are brittle in nature, apart from TTT (100 wt%), it has some ductility, since it does not abruptly break, like the others. The adhesive strengths of these samples are recorded in *Table A.1, A.2*. The area under

9

this curve represents the energy absorbed by the adhesive, which is also known as the adhesive energy [J]. The adhesive energy values are also recorded in the previously mentioned tables.

Due to the time constraints of this project, testing was limited to G1/G21 1:1 and 50 wt% adhesives on PAMA coated glass surfaces. Only G21 1:1 adhesives were tested on uncoated and PAMA coated aluminum and polycarbonate surfaces.
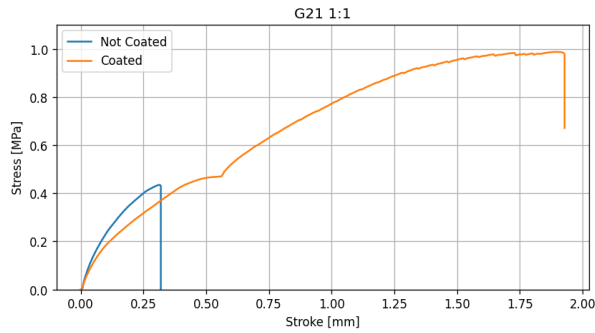
Figure 3.8: Stress - strain curve of G21 1:1 on glass surfaces.

Figure 3.8 shows the sample stress-strain curve for the G21 1:1 adhesive on both uncoated and PAMA-coated glass surfaces, represented by the blue and orange curves, respectively. It can be seen that the maximum stress at which the adhesive fails for the coated sample is higher than the uncoated sample, suggesting that the iCVD PAMA coating improves the strength. However, a more in-depth statistical analysis is required to make that statement. For now, the stress-strain curves were analysed for the characteristics of the adhesive failure.

The uncoated stress-strain curves (*Figures 3.7 & B.3*) have a linear increase in stress as the sample was sheared and the adhesive fails abruptly at the maximum stress, apart from TTT (100 wt%). Similarly, for the G21 1:1 PAMA coated sample, the stress increases linearly as it was sheared, and it fails abruptly at the maximum stress. However, the PAMA coated curve possesses a temporary reduction around a similar stress value as the maximum stress of the uncoated G21 1:1 sample.

This temporary reduction in stress could be likely due to the weak secondary bonds breaking at the adhesive interface. This is consistent with why the temporary reduction is at a similar stress value as the maximum stress for the uncoated sample. After the weak secondary bonds have broken, the stress then must have redistributed over the remaining primary bonds, which were the C-S bonds after the polymerisation between the PAMA coating at the adhesive bulk. These primary bonds continue to bear the stress, until all the primary and secondary bonds at the adhesive interface and cohesive bulk break, resulting in the abrupt snapping of the adhesive.

Similar behaviour in stress has been observed by

Machalická & Eliášová, 2017[32] and Qi et al., 2018[33]. Machalická & Eliášová, 2017 attributed this to thick adhesive layers, which lead to an increase in the formation of microcracks and voids, resulting in the temporary reduction in stress for their UV cured adhesive joints in glass structures. Qi et al., 2018 investigated epoxy resins made from various ratios of epoxidised soybean oil (ESO) and tannic acid (TA). The temporary reductions in stress were observed only in samples with lower TA content, which corresponds to a lower amount of -OH functional groups present. This could likely suggest that many ESO molecules did not participate in the network, allowing for chain relaxation/disentanglement under stress, leading to the observed temporary reduction in stress. In contrast, samples with higher TA content did not display these temporary reductions in stress because the network was highly rigid, preventing ESO chains from relaxing or disentangling.

(a) Uncoated.   **(b) PAMA coated.**
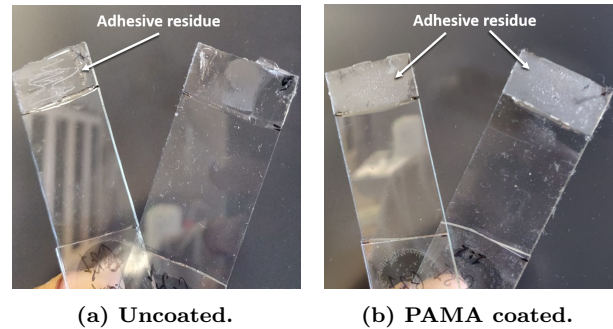
Figure 3.9: Lap shear sample images of G21 1:1 on glass surface after failure.

Figure 3.9, show the failed lap shear samples of G21 1:1 on a glass surface, on the left is the uncoated glass and on the right is the PAMA coated glass. The uncoated sample has adhesive residue on only one surface, the other surface has little to no adhesive, suggesting that it is an adhesive break. Whereas, the PAMA coated sample has adhesive residue on both sides, suggesting a cohesive break. Connecting this back to the stress-strain curve(*Figure 3.8*). For the uncoated sample, since there was no possibility of forming the strong primary bonds between the surface and the adhesive bulk, only the secondary bonds, such as London dispersion forces, dipole-dipole bonding or mechanical interlocking were responsible for the adhesive strength.

These forces are relatively weak compared to the bonding strength of a primary bond, such as the C-S, which occurs between the PAMA coating and the adhesive bulk. Hence the weak secondary bonds in uncoated sample are broken, resulting in the adhesive failure seen in *Figure 3.9a*, and the corresponding blue stress-strain curve is seen.

It is likely that the coating and the bulk adhesive did not completely bond with each other, thereby some secondary bonds were still responsible for the adhesive strength at the adhesive interface. And since

they are weaker than the primary bonds, they break first, resulting in a temporary reduction in stress. Reddy et al., 2008[34] critically analysed the Termonia and Smith model[35] which explores the stress redistribution from Van der Waals forces (secondary forces) to intramolecular forces (primary forces) that leads to the temporary reduction in stress.

The remaining bonds continue to bear the stress, until the cohesive primary and secondary bonds fail, resulting in the cohesive failure, seen in *Figure 3.9b*. The previously mentioned statements were similarly seen for G1 1:1 samples for glass surfaces, *Figure B.4*. However, to fully confirm the mode of failure, microscopic techniques such as SEM or AFM are needed.
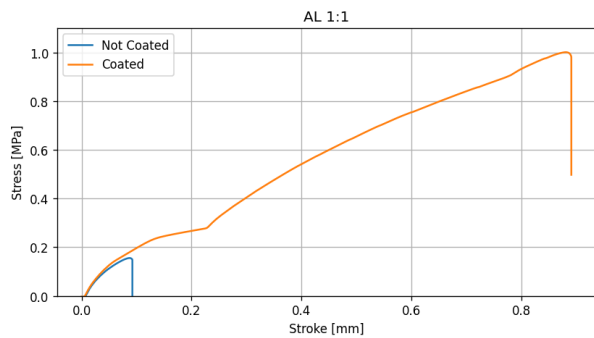
Figure 3.10: Stress - strain curve of G21 1:1 on PAMA coated aluminium-glass surfaces.
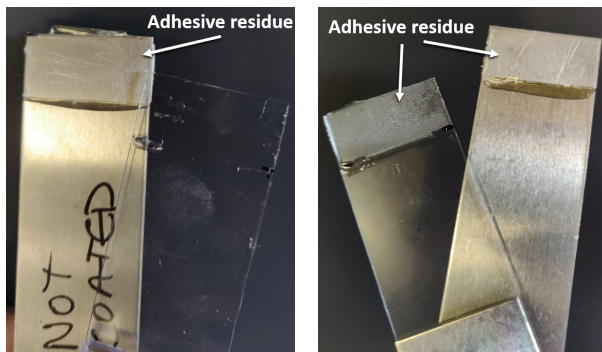
(a) Uncoated.   (b) PAMA coated.

Figure 3.11: Lap shear images of G21 1:1 on aluminium-glass surfaces after failure.

G21 1:1 adhesive on uncoated and PAMA coated aluminium-glass surfaces[‡] respond similar to the glass surfaces. In *Figure 3.10*, uncoated curve has a small maximum stress, and an abrupt break, whereas the coated curve, has the same temporary reduction in stress as seen in the G21 1:1 glass sample as well. The sample images, *Figure 3.11*, also show similar cohesive and adhesive failure for uncoated and coated samples respectively.

[‡]The reason for using aluminium-glass surfaces was that the adhesive was cured upon irradiation of UV light, hence at least one of the surfaces had to be UV transparent, and to be consistent the same approach was take for polycarbonate
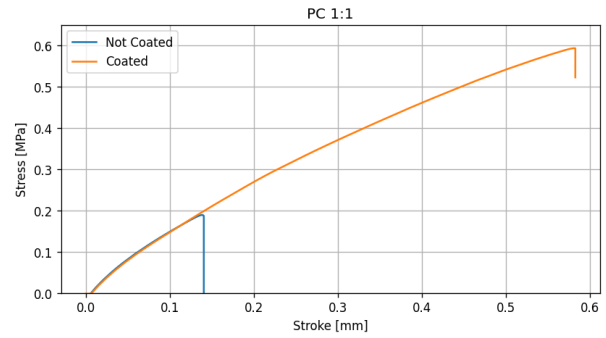
Figure 3.12: Stress - strain curve of G21 1:1 on PAMA coated polycarbonate-glass surfaces.

Polycarbonate-glass samples were a bit different from the glass and aluminium-glass samples. This difference can be noted in the stress-strain curve of G21 1:1 on uncoated and PAMA coated polycarbonate-glass surface, *Figure 3.12*. The PAMA coated stress-strain curve (orange), does not possess a temporary reduction in stress as the aforementioned stress-strain curves did. This could likely suggest that the PAMA coating contribution was minimal, and thus no redistribution is seen as not enough primary bonds were available to bear the stress once the secondary bonds failed.
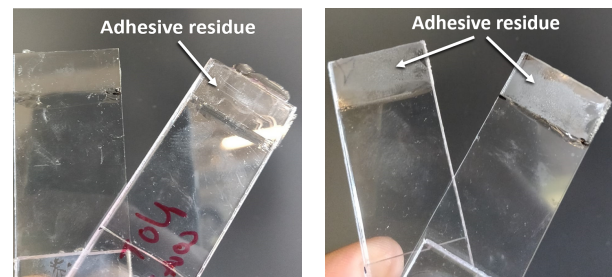
(a) Uncoated.   (b) PAMA coated.

Figure 3.13: Lap shear images of G21 1:1 on polycarbonate-glass surfaces after failure.

However, this does not agree with the polycarbonate-glass sample images for the G21 1:1 adhesive, *Figure 3.13*. Cohesive and adhesive failure is seen for the polycarbonate-glass uncoated and coated samples respectively. Since the PAMA coated sample, experienced a cohesive failure, it does not correlate with what is seen for the coated glass and aluminium-glass surfaces, as those possess the temporary reduction in the stress-strain curve.

Thus, it is mostly likely that there was an inefficient use of coating, not all the allyl groups participated, and further microscopic analysis is required. The reason for the participation of lesser number of allyl groups could be because of the PAMA coating and the polycarbonate surface have a poor interaction relative to the interactions between PAMA coating and glass or aluminium.

---

samples.

It is likely that the polycarbonate surfaces are very smooth, hence few ridges are available for the coating to interlock, hence lower allyl groups present than glass or aluminium surfaces.

If fewer allyl groups were present on the surface, then there would have been an excess of SH groups in the adhesive bulk, this would have caused a denser crosslinking network to be formed, as now SH groups were in excess, thereby maximising the involvement of TTT in the bulk. This leads to a more brittle adhesive bulk, thus more prone to crack propagation, which explains the stress-strain curve and the cohesive failure sample image, *Figure 3.13b*. A theoretical calculation of the effective contribution of PAMA coating related to the previous discussion is provided in *Appendix C* to understand the relationship between stress-strain curves and the bond energies in the adhesive system, refer to *Table C.1*.
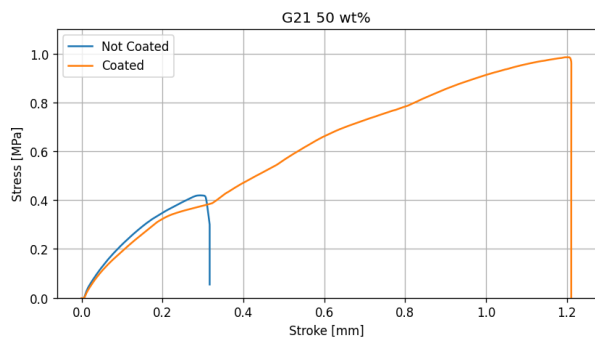
Figure 3.14: Stress - strain curve of G21 50 wt% on PAMA coated glass surface.

In addition to the G21 1:1 adhesive on glass surfaces, G21 50 wt% was also tested. The stress-strain curve for the adhesive is seen above, *Figure 3.14*. The curves are similar in nature to the previously mentioned- linear increase of stress and an abrupt failure, suggesting brittleness. However, instead of possessing one temporary reduction in stress, the higher crosslinker content results in another temporary reduction in stress at a higher stress value. The likely reason for this is counter-intuitive to the polycarbonate-glass surface. Since there is a higher crosslinker content available in the bulk, the SH groups of the polysulphide are used up in the bulk, thus limiting the amount for the polymerisation with the PAMA coating.

Therefore, the second temporary reduction in stress is suggested to be another temporary stress reduction. Because there is an even lower amount of primary bonding between the surface and the bulk, the first set of weak secondary bonds fail, resulting in the first temporary reduction. Afterwards, the stress is redistrbuted and the sample is continued to be sheared, as the load gets larger, the second set of weak secondary bonds fail, resulting in the second temporary reduction, but at a higher stress value. Finally, the load reaches such a stress value that the whole adhesive system can no longer bear it and it

fails at the maximum stress. The sample images for G21 50 wt% on glass surfaces were same as the sample images that were obtained as G21 1:1 on glass surfaces, *Figure 3.9*. The previously mentioned statements were also true for G1 1:1 50 wt%, *Figure B.5*.

Another possible theory to explain the temporary reduction in stress involves the disentanglement and relaxation of long polysulfide chains (as shown in *Figure 1.5*). During this process, the relaxation of these chains results in a temporary decrease in stress. The energy is initially expended in disentangling the chains, rather than in breaking bonds. Once the chains are disentangled, the energy resumes back to breaking the bonds, eventually leading to the failure of the adhesive, at its maximum stress. The redistribution of stress in polymer networks is explored by Tauber et al., 2021[36] via coarse-grained simulations of polymer networks.

Yige et al., 2024[37], studied the stress redistribution adhesive layer (SRAL) in high energy density flexible batteries. They also observed similar temporary reductions in stress-strain curves after the addition of flexible polyurethane. Similarly, Abdellah et al., 2021[38] also observed the same temporary reduction in stress due to the addition of glass fibres. The reason for the temporary reduction in their paper was due to the "pulling" of the glass fibres. All the previous references can be used to understand stress reduction and redistribution due to relaxation or disentanglement of chains/fibres.

3.4 Adhesive Strength Analysis

The previous section focused on analysing the stress-strain curves and the failed visual images of the adhesives. However, that analysis does not provide any statistical understanding of the effects of PAMA-coated surfaces and different cross-linker content on the adhesive strength. Hence, this section will focus on the statistical analysis with the help of ANOVA with a post-hoc Tukey HSD test.

Boxplots were plotted to understand the distribution of the data obtained. Red dots, blue dots and the letters correspond to the mean value, outliers and statistical significance letters respectively. The significant letters are obtained from the Tukey HSD test, which identifies if two sets of data overlap within the 95% confidence interval, to visualise this easier, the letters are provided. Boxplots labelled with the same letters indicate that the differences between them are not statistically significant, meaning their p-values are greater than 0.05. If boxplots are statically not significant from each other, then they have similar adhesive strengths.

Figure 3.15, represents the adhesive strength for the various crosslinker amount. By only observing the mean values, the adhesive strength increases as the amount of crosslinker is increased, but then
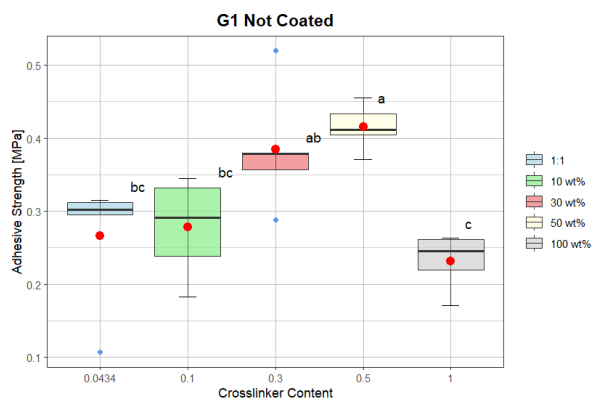
Figure 3.15: Boxplot of G1 for different crosslinker amounts on uncoated glass surfaces.
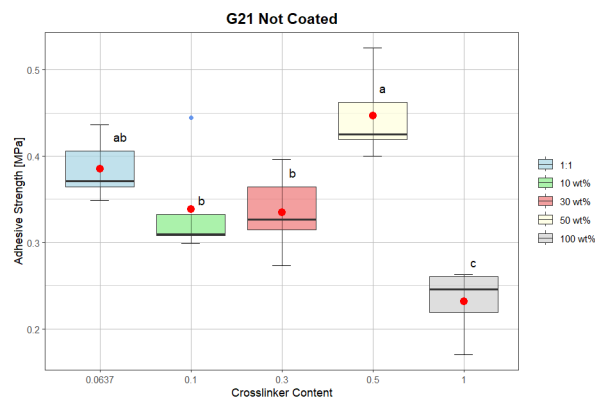
Figure 3.16: Boxplot of G21 for different crosslinker amounts on uncoated glass surfaces.

decreases as too much crosslinker is added, which is seen with the steep decrease in adhesive strength of TTT (100 wt%). However, statistically, this trend is not true. 1:1, 10 wt% & 30% have similar adhesive strength, hence the adhesive strength is constant over these crosslinker amounts. At around 30 wt% and 50 wt% the adhesive strength increases slightly, and increasing the crosslinker amount to 100 wt% results in an adhesive strength similar to the 1:1 and 10 wt%.

Table 3.1: SH:ENE molar ratios of the weight percentages for G1 and G21.

Crosslinker	SH : ENE ratio	
Content	G1	G21
10 wt%	1:3	1:2
30 wt%	1:10	1:6
50 wt%	1:22	1:15

Converting the weight percentages into molar ratios with the help of *Equations 2.1, 2.2 & 2.3* helps explain why the 1:1, 10 wt% and 30 wt% may have similar adhesive strengths. *Table 3.1*, shows the molar ratio of SH:ENE for the corresponding weight percentages for G1 and G21. The molar ratios of the 1:1 for G1 are quite similar to 10 wt% (1:3) and 30 wt% (1:10), thus could explain why the adhesive strengths are similar.

The boxplot of G21 for different crosslinker amounts, *Figure 3.16*, results in a similar plot as G1. 1:1, 10 wt% and 30 wt% have similar adhesive strengths. This is also explained by the fact that the molar ratios of these are quite similar.

The 100 wt% adhesive is only the crosslinker TTT. It has the lowest adhesive strength, which agrees with the FTIR plot of TTT, *Figure 3.6*. As confirmed before, there is no reaction observed between the TTT molecules. Hence, it is understandable that the adhesive strength is significantly lower, as the only forces responsible are the secondary bonding forces. However, 100 wt% is comparable in strength to G1 1:1 and 10wt%, but is different from G21

1:1 and 10 wt%. The reason for this might be that G1 has a higher viscosity relative to G21, see *Figure B.6*. High viscosity leads to poor mobility of the molecules, hence it is difficult for the SH and ENE functional groups to find each other and react. Additionally, G1 has a lower SH content than G21, hence G1 is less reactive than G21. Thus, explaining the poor strength of G1 1:1 and 10 wt%

Moreover, in *Figure 3.16* 1:1 and 50 wt% have similar adhesive strength, this is opposite of what is happening in G1, *Figure 3.15*. The reason for this is that adding more TTT to the polysulphides reduces the viscosity, as the sterically hindered TTT molecules break apart the interactions between the long polysulphide chains. Hence G21 1:1 has higher viscosity than G21 50 wt%, note G21 also has relatively high reactivity due to more SH groups present.

Thus, it is possible that local agglomeration of crosslinking is occurring, since the mobility is low due to higher viscosity and the reactivity is high, the thiol-ene reaction is occurring in close domains that are spread across the adhesive bulk. The result of these crosslinker agglomerations could actually increase the stress bearing capacity of the adhesive, as potential propagating cracks could be stopped due to the presence of these agglomeration. Thereby resulting in similar adhesive strength to 50 wt% where the viscosity is lower and crosslinker amount is higher, thus the possibility of a more homogeneous crosslinking density is favored, which results in also a high adhesive strength.

Kallungal et al., 2022[39] present the impact of carbon black agglomeration in an elastomer. They observe that the presence of the agglomerations results in deviation of the crack from the original path, reduced crack propagation speed and crack arrest. Thus, showcasing that presence of agglomeration allows for resistant in crack propagation and an increase in adhesive strength. However, while Kallungal et al. experimented with carbon black as the agglomerate, this study proposes that there might be regions of non-homogenous crosslinking present in the matrix.

A final point of discussion about the 100 wt% adhesive for the uncoated samples is that even though the 100 wt% adhesive doesn't polymerise, it seems to still have a considerable about of adhesive strength. It is likely due to the fact that 100 wt% is significantly lower in viscosity than the other adhesives, hence it had a higher wettability. Additionally, TTT's melting point is around 25°C, at the room temperature of 15°C it is a solid.

Thus, even though the 100 wt% adhesive, which is mostly TTT, does not cure, it however does solidify after seeping into the cracks of the surface, allowing for mechanical interlocking. This could potentially explain why it still has some adhesive strength. Moreover, it also provides insight into the stress-strain curve of 100 wt%, *Figure 3.7*. 100 wt% does not have an abrupt break, however, it behaves with a plastic nature. This plastic nature after the maximum stress could likely be due to the melting of the frozen TTT, as the temperature increases because of the molecules shearing against each other.
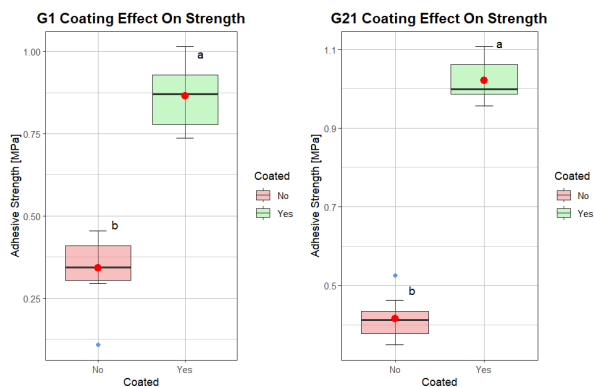
Figure 3.17: Boxplot of G1 and G21 coating effect on adhesive strength.

Figure 3.17 represents the uncoated and PAMA coated glass surfaces for G1 and G21[§]. There is a significant increase in the adhesive strength after the surface is PAMA coated for both G1 and G21. Therefore, the surface modification of iCVD PAMA coating statistically improves the adhesive strength of the system. Additionally, G1 and G21 have different responses in adhesive strength to the PAMA coating. In *Figure 3.17*, the G21 adhesive strength difference between the uncoated and coated is higher than in the G1 adhesive strength difference. Therefore, G21 polysulphide outperforms G1 after the glass surface is coated with PAMA.

Figure 3.18 compares the only the G1 and G21 adhesive on PAMA coated glass surface. The boxplot also confirms that G21 does indeed statistically outperform G1.

Finally, *Figure 3.19* represents the adhesive strengths of G21 1:1 on uncoated and PAMA coated glass, aluminium and polycarbonate surfaces. For

Figure 3.18: Boxplot comparing coating effectiveness of G1 & G21 .
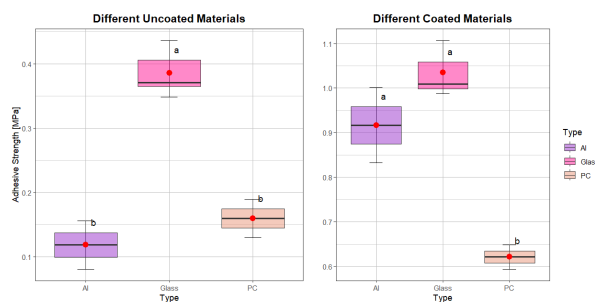
Figure 3.19: Boxplot of G21 1:1 on glass, aluminium and polycarbonate coating effects.

uncoated surfaces, glass surpasses aluminium and polycarbonate significantly. Aluminium and polycarbonate have similar adhesive strength. Glass likely has a higher surface energy than aluminium and polycarbonate. After PAMA coating, the adhesive strength of glass and aluminium become statistically similar. However, polycarbonate has relatively lower adhesive strength compared to the other two. Nevertheless, the PAMA coating is effective in enhancing the adhesive strength on polycarbonate surfaces as well.

The relatively lower adhesive strength of polycarbonate to the other two surfaces agrees with the aforementioned discussion of the stress-strain curve, as it did not possess the temporary reduction in stress. Hence, it can be likely said that the PAMA coating on the polycarbonate surface is being used inefficiently, not all allyl groups on the surface are reacting with the SH groups in the adhesive bulk. It is also backed up with the theoretical calculations, refer to *Appendix C*.

4   Future Perspectives

There are several unexplored directions for the future of the research. Firstly, utilising Raman spectroscopy to analyze the change in intensity of thiol functional groups during polymerization would be advantageous, as FTIR is not sensitive enough to detect the thiol

---

[§]The data for the uncoated and coated is composed of 1:1 and 50 wt%.

peaks, this also applies for the ene groups as well. Additionally, it may be possible to follow the polymerisation in *situ* with Raman spectroscopy.

Secondly, due to the time constraint on the research, a small amount of data was gathered, and the sample size might be too small to make generalised statements about the entire population. Hence, more data collection is required, and various other crosslinker amounts need to be tested, such as 60 wt%, 70 t%, 80 wt% and 90 wt%. Testing these crosslinker contents may provide new insight into the interplay between the viscosity and SH content.

Thirdly, new surfaces similar to polycarbonate could be tested to understand the surface interactions between such surfaces and the adhesive. It remains unclear whether the poor interaction is between the adhesive and the PAMA coating on the polycarbonate surface, or between the PAMA coating and the polycarbonate surface itself.

Finally, techniques such as SEM, AFM, and XPS need to be conducted on cross-sections of the failed samples to identify the type of failure that occurred. Furthermore, with the help of these techniques, it might be possible to check the theory of agglomeration in the adhesive bulk for G21 1:1, or other adhesives.

5   Conclusion

In conclusion, the surface modified iCVD PAMA coating did indeed absorb onto surfaces and polymerise, this was confirmed with the analysis of an SEM image and FTIR analysis. Additionally, the light induced thiol-ene click reaction between the polysulphides and crosslinker TTT was occurring, it was analysed via FTIR. Subsequently, it was observed that TTT did not polymerise with itself. From the lap shear tests, the stress-strain curves were analysed to understand the failure response of the adhesive, it was observed that the adhesives were brittle apart from the 100 wt%.

Additionally, the curves had temporary reductions in stress, these were theorised to be due to the breaking of weaker secondary bonds or the relaxations of the polysulphide chains. With the help of ANOVA and Tukey HSD, the adhesive strengths of different categories could be statistically compared with a 95% confidence interval. It was observed that for uncoated glass samples, G1 1:1 10 wt% and 30 wt% had similar adhesive strengths, however, G21 had the opposite results. G21 1:1 and 50 wt% also had similar adhesive strength, it was theorised that it was due to agglomeration in the adhesive bulk of G21 1:1, and the interplay between viscosity and crosslinker content.

Furthermore, it was observed with statistical significance that the PAMA coating enhances the adhesive strength of G1 and G21 adhesives on glass,

aluminium, and polycarbonate surfaces. Moreover, it was noticed that G21 outperforms G1, due to lower viscosity and higher SH content, allowing the G21 polysulphide to be relatively more mobile and reactive than G1. Additionally, polycarbonate surfaces were identified to be lower in adhesive strength than glass and aluminium, it was likely due to the interactions between the adhesive and PAMA coated polycarbonate surface, or the interaction between the PAMA coating and polycarbonate surface itself. Theoretical calculation of the effectiveness of PAMA coating was conducted to further support the theory.

Throughout this research, it has been identified that the adhesive systems exhibit a complex interplay between the viscosity, crosslinker content and SH content. However, the research has resulted in interesting findings of this interplay which will help to lay a foundation for upcoming projects.

6   Acknowledgements

References

(1) Mazza, P. P. A.; Martini, F.; Sala, B.; Magi, M.; Colombini, M. P.; Giachi, G.; Landucci, F.; Lemorini, C.; Modugno, F.; Ribechini, E. A new Palaeolithic discovery: tar-hafted stone tools in a European Mid-Pleistocene bone-bearing bed. *Journal of Archaeological Science* **2006**, *33*, 1310–1318, DOI: `https://doi.org/10.1016/j.jas.2006.01.006`.

(2) Skeist, I., *Handbook of adhesives*, 3rd ed.; Van Nostrand Reinhold: New York, 1990.

(3) Benedek, I., *Pressure-sensitive adhesives and applications.* 2nd ed.; Marcel Dekker: New York, 2004.

(4) Drew, R. Adhesive tape, 1930.

(5) Bishopp, J. Adhesives for Aerospace Structures. *Elsevier eBooks* **2011**, 301–344, DOI: `https://doi.org/10.1016/b978-1-4377-4461-3.10013-6`.

(6) Wake, W. Theories of adhesion and uses of adhesives: a review. *Polymer* **1978**, *19*, 291–308, DOI: `https://doi.org/10.1016/0032-3861(78)90223-9`.

(7) Ohara, T.; Sato, T.; Shimizu, N.; Prescher, G.; Schwind, H.; Weiberg, O.; Marten, K.; Greim, H.; Shaffer, T. D.; Nandi, P. Acrylic Acid and Derivatives. *Ullmann's Encyclopedia of Industrial Chemistry* **2020**, 1–21, DOI: `https://doi.org/10.1002/14356007.a01_161.pub4`.

(8) Mattson, G. K.; Conklin, E. G.; Desai, S.; Nielander, G.; Savage, M.; Morgensen, S. A practical approach to crosslinking. *Molecular Biology Reports* **1993**, *17*, 167–183, DOI: `https://doi.org/10.1007/bf00986726`.

(9) Yagci, Y.; Jockusch, S.; Turro, N. J. Photoinitiated Polymerization: Advances, Challenges, and Opportunities. *Macromolecules* **2010**, *43*, 6245–6260, DOI: `https://doi.org/10.1021/ma1007545`.

(10) Tsuji, Y. Molecular Understanding of the Distinction between Adhesive Failure and Cohesive Failure in Adhesive Bonds with Epoxy Resin Adhesives. *Langmuir* **2024**, DOI: `https://doi.org/10.1021/acs.langmuir.3c04015`.

(11) Neděla, O.; Slepička, P.; Švorčík, V. Surface Modification of Polymer Substrates for Biomedical Applications. *Materials* **2017**, *10*, 1115, DOI: `https://doi.org/10.3390/ma10101115`.

(12) Tenhaeff, W. E.; Gleason, K. K. Initiated and Oxidative Chemical Vapor Deposition of Polymeric Thin Films: iCVD and oCVD. *Advanced Functional Materials* **2008**, *18*, 979–992, DOI: `https://doi.org/10.1002/adfm.200701479`.

(13) Yu, S. J. et al. Initiated Chemical Vapor Deposition: A Versatile Tool for Various Device Applications. *Advanced Engineering Materials* **2017**, *20*, DOI: `https://doi.org/10.1002/adem.201700622`.

(14) Kolb, H. C.; Finn, M. G.; Sharpless, K. B. Click Chemistry: Diverse Chemical Function from a Few Good Reactions. *Angewandte Chemie International Edition* **2001**, *40*, 2004–2021, DOI: `https://doi.org/10.1002/1521-3773(20010601)40:11%3C2004::aid-anie2004%3E3.0.co;2-5`.

(15) Northrop, B. H.; Coffey, R. N. Thiol–Ene Click Chemistry: Computational and Kinetic Analysis of the Influence of Alkene Functionality. *Journal of the American Chemical Society* **2012**, *134*, 13804–13817, DOI: `https://doi.org/10.1021/ja305441d`.

(16) Resetco, C.; Hendriks, B.; Badi, N.; Du Prez, F. Thiol–ene chemistry for polymer coatings and surface modification – building in sustainability and performance. *Mater. Horiz.* **2017**, *4*, 1041–1053, DOI: `https://doi.org/10.1039/c7mh00488e`.

(17) Turro, N. J.; Scaiano, J. C.; Ramamurthy, V., *Principles of molecular photochemistry*; University Science Books: Sausalito, CA, 2009.

(18) Pappas, S. P., *UV Curing*; Technology Marketing Corp: 1978; Vol. 2.

(19) Pickett, J. Weathering of Plastics. *Handbook of Environmental Degradation of Materials* **2018**, *1*, 163–184, DOI: `https://doi.org/10.1016/B978-0-323-52472-8.00008-3`.

(20) Decker, C. The use of UV irradiation in polymerization. *Polymer International* **1998**, *45*, 133–141, DOI: `https://doi.org/10.1002/(sici)1097-0126(199802)45:2%3C133::aid-pi969%3E3.0.co;2-f`.

(21) Aubert, S.; Bezagu, M.; Spivey, A. C.; Arseniyadis, S. Spatial and temporal control of chemical processes. *Nature Reviews Chemistry* **2019**, *3*, 706–722, DOI: `https://doi.org/10.1038/s41570-019-0139-6`.

(22) Ebe, K.; Seno, H.; Horigome, K. UV curable pressure-sensitive adhesives for fabricating semiconductors. I. Development of easily peelable dicing tapes. *Journal of applied polymer science* **2003**, *90*, 436–441, DOI: `https://doi.org/10.1002/app.12673`.

(23) Kulkarni, S.; Sharma, A.; Swamy, K. V. Effect of Photoactivation by Ultraviolet Light on Bond Strength of Composite Veneer on Stainless Steel Crowns—An In Vitro Study. *International Journal of Clinical Pediatric Dentistry* **2019**, *12*, 50–52, DOI: `https://doi.org/10.5005/jp-journals-10005-1593`.

(24) Decker, C. Photoinitiated crosslinking polymerisation. *Progress in Polymer Science* **1996**, *21*, 593–650, DOI: `https://doi.org/10.1016/0079-6700(95)00027-5`.

(25) Schwalm, R. Photoinitiators and Photopolymerization. *Encyclopedia of Materials: Science and Technology* **2001**, 6946–6951, DOI: `https://doi.org/10.1016/b0-08-043152-6/01230-4`.

(26) Ravve, A. Step-Growth Polymerization and Step-Growth Polymers. *Springer eBooks* **2012**, 403–535, DOI: `https://doi.org/10.1007/978-1-4614-2212-9_7`.

(27) Zhang, W.; Douglas, J. F.; Starr, F. W. How Dispersity from Step-Growth Polymerization Affects Polymer Dynamics from Coarse-Grained Molecular Simulations. *Macromolecules* **2022**, *55*, 9901–9907, DOI: `https://doi.org/10.1021/acs.macromol.2c01623`.

(28) Chan, C. H.; Chen, J.-T.; Farrell, W. S.; Fellows, C. M.; Keddie, D. J.; Luscombe, C. K.; Matson, J. B.; Merna, J.; Moad, G.; Russell, G. T.; Théato, P.; Topham, P. D.; Vargas, L. S. Reconsidering terms for mechanisms of polymer growth: the "step-growth" and "chain-growth" dilemma. *Polymer Chemistry* **2022**, *13*, 2262–2270, DOI: `https://doi.org/10.1039/D2PY00086E`.

(29) Nouryon Thioplast Ⓡ G Polysulfides `https://www.nouryon.com/globalassets/inriver/resources/brochure-thioplast-g-global-en.pdf`.

(30) Im, S. G.; Bong, K. W.; Lee, C.-H.; Doyle, P. S.; Gleason, K. K. A conformal nano-adhesive via initiated chemical vapor deposition for microfluidic devices. *Lab Chip* **2009**, *9*, 411–416, DOI: `https://doi.org/10.1039/b812121d`.

(31) Lancaster, J., *Metallurgy of Welding*, 6th ed.; Woodhead Publishing: Sawston, United Kingdom, 1999, pp 76–77.

(32) Machalická, K.; Eliášová, M. Adhesive joints in glass structures: effects of various materials in the connection, thickness of the adhesive layer, and ageing. *International Journal of Adhesion and Adhesives* **2017**, *72*, 10–22, DOI: `https://doi.org/10.1016/j.ijadhadh.2016.09.007`.

(33) Qi, M.; Xu, Y.-J.; Rao, W.-H.; Luo, X.; Chen, L.; Wang, Y.-Z. Epoxidized soybean oil cured with tannic acid for fully bio-based epoxy resin. *RSC Advances* **2018**, *8*, 26948–26958, DOI: `https://doi.org/10.1039/c8ra03874k`.

(34) Reddy, B. K.; Estevez, R.; Basu, S. Revisiting the mesoscopic Termonia and Smith model for deformation of polymers. *Modelling and simulation in materials science and engineering* **2008**, *16*, 025008–025008, DOI: `https://doi.org/10.1088/0965-0393/16/2/025008`.

(35) Termonia, Y.; Smith, P. Kinetic model for tensile deformation of polymers. *Macromolecules* **1987**, *20*, 835–838, DOI: `https://doi.org/10.1021/ma00170a023`.

(36) Tauber, J.; Rovigatti, L.; Dussi, S.; Jasper Sharing the Load: Stress Redistribution Governs Fracture of Polymer Double Networks. *Macromolecules* **2021**, *54*, 8563–8574, DOI: `https://doi.org/10.1021/acs.macromol.1c01275`.

(37) Xiong, Y.; Wang, Z.; Yan, X.; Li, T.; Jing, S.; Hu, T.; Jin, H.; Liu, X.; Kong, W.; Huo, Y.; Ge, X. Elastic Polyurethane as Stress-Redistribution-Adhesive-Layer (SRAL) for Directly Integrated High-Energy-Density Flexible Batteries. *Advanced science* **2024**, DOI: `https://doi.org/10.1002/advs.202401635`.

(38) Abdellah, M. Y.; Alfattani, R.; Alnaser, I. A.; Abdel-Jaber, G. T. Stress Distribution and Fracture Toughness of Underground Reinforced Plastic Pipe Composite. *Polymers* **2021**, *13*, 2194, DOI: `https://doi.org/10.3390/polym13132194`.

(39) Kallungal, J.; Chazeau, L.; Chenal, J.-M.; Adrien, J.; Maire, E.; Barrès, C.; Cantaloube, B.; Heuillet, P.; Wilde, F.; Moosmann, J.; Weitkamp, T. Crack propagation in filled elastomers: 3D study of mechanisms involving the filler agglomerates. *Engineering Fracture Mechanics* **2022**, *274*, 108771, DOI: `https://doi.org/10.1016/j.engfracmech.2022.108771`.

(40) `https://gchem.cm.utexas.edu/data/section2.php?target=bond-energies-table4.php`.

A Appendix

Table A.1: G1 uncoated.

Average	1:1	10 wt%	30 wt%	50 wt%	100 wt%
Adhesive Strength [MPa]	0.266	0.278	0.385	0.415	0.232
Adhesive Energy [J]	0.011	0.010	0.022	0.033	0.008

Table A.2: G21 uncoated.

Average	1:1	10 wt%	30 wt%	50 wt%	100 wt%
Adhesive Strength [MPa]	0.385	0.339	0.335	0.447	0.232
Adhesive Energy [J]	0.017	0.018	0.016	0.033	0.008

Table A.3: G1 & G21 PAMA coated.

	G1		G21	
Average	1:1	50 wt%	1:1	50 wt%
Adhesive Strength [MPa]	0.795	0.935	1.03	1.01
Adhesive Energy [J]	0.181	0.267	0.387	0.244

Table A.4: Aluminium & polycarbonate G21 1:1. Uncoated and PAMA coated.

	Uncoated		Coated	
Average	Al	PC	Al	PC
Adhesive Strength [MPa]	0.118	0.159	0.844	0.639
Adhesive Energy [J]	0.002	0.004	0.124	0.068

B   Appendices
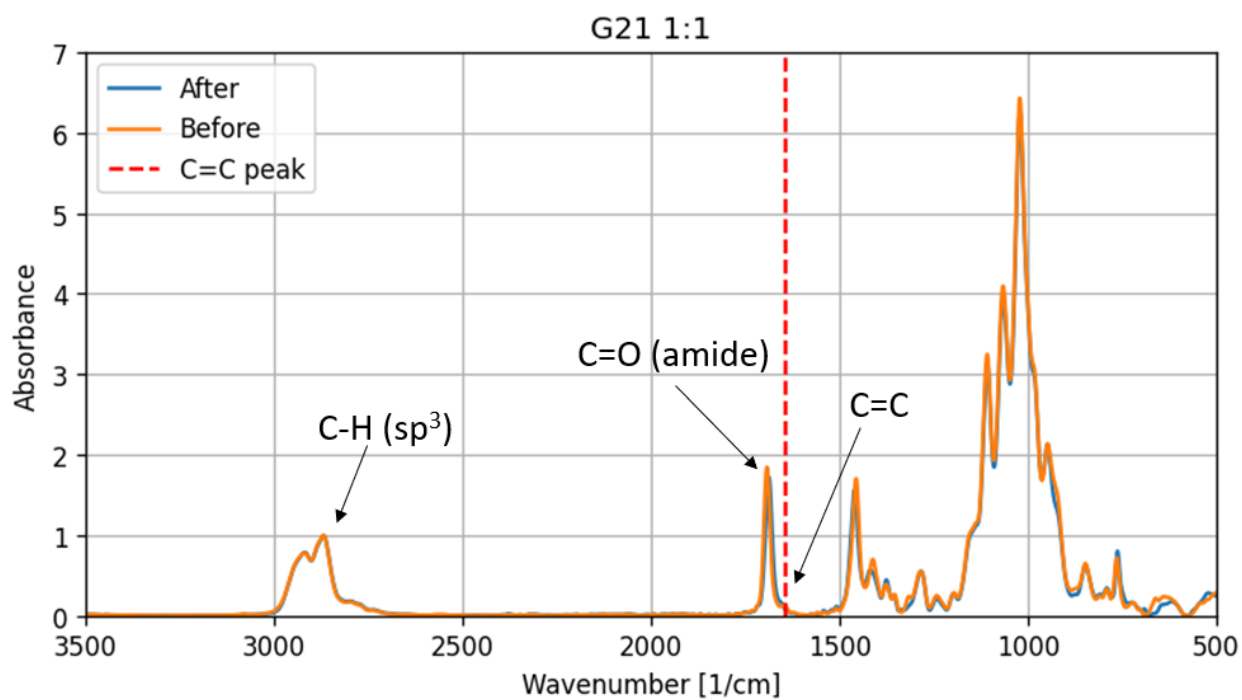
Figure B.1: FTIR plot of G21 1:1 adhesive before (orange) and after (blue) curing. The red dashed line indicates the C=C peak.
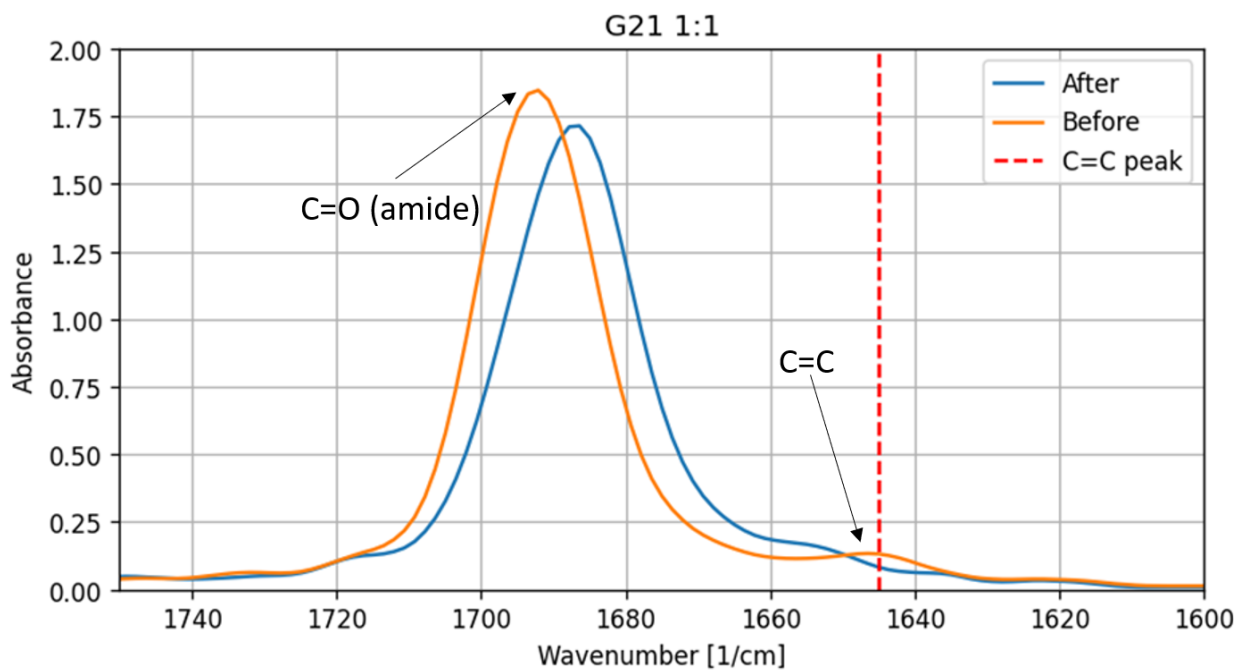
Figure B.2: Zoomed FTIR plot of G21 1:1 in the 1740 - 1600 cm^{-1} region.
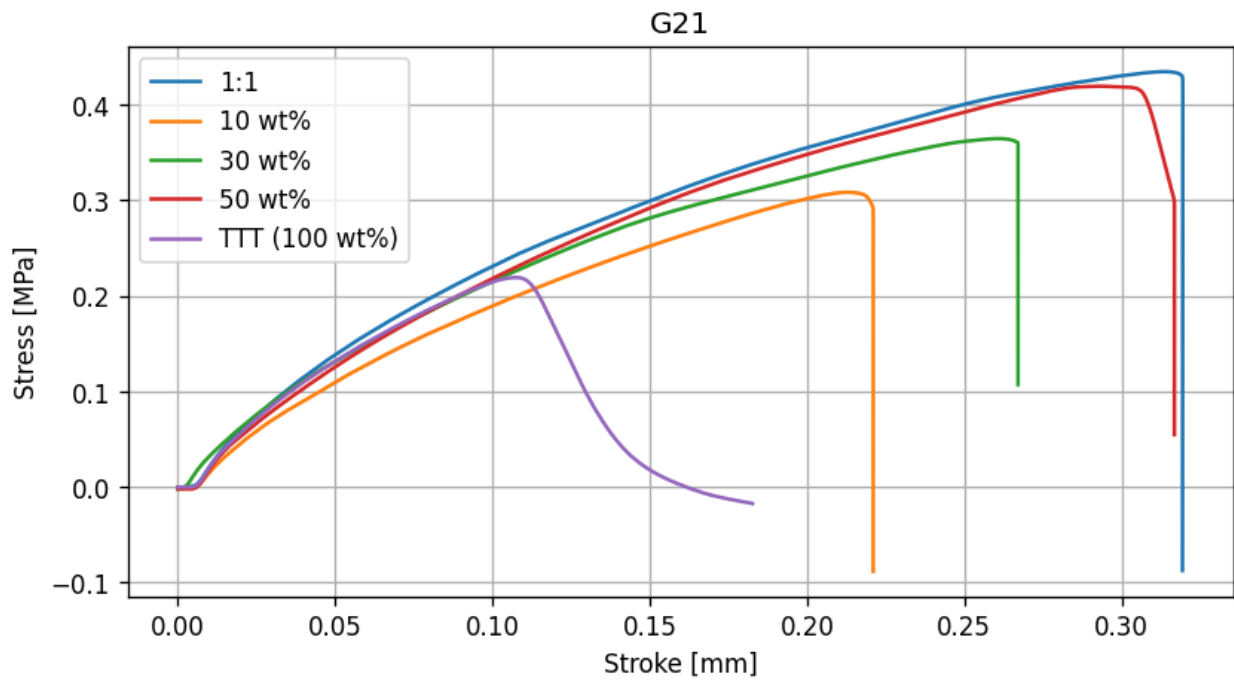
Figure B.3: Stress - strain curve of G21 uncoated for different crosslinker amounts.
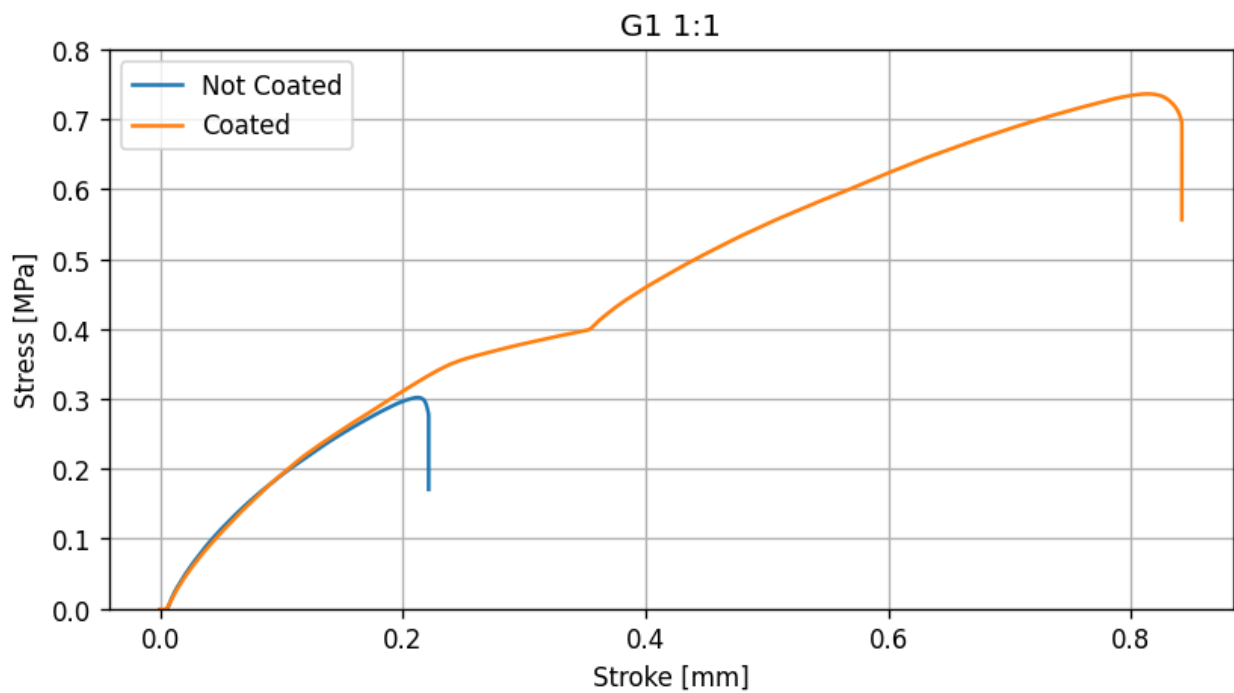
Figure B.4: Stress - strain curve of G1 1:1 uncoated and PAMA coated.
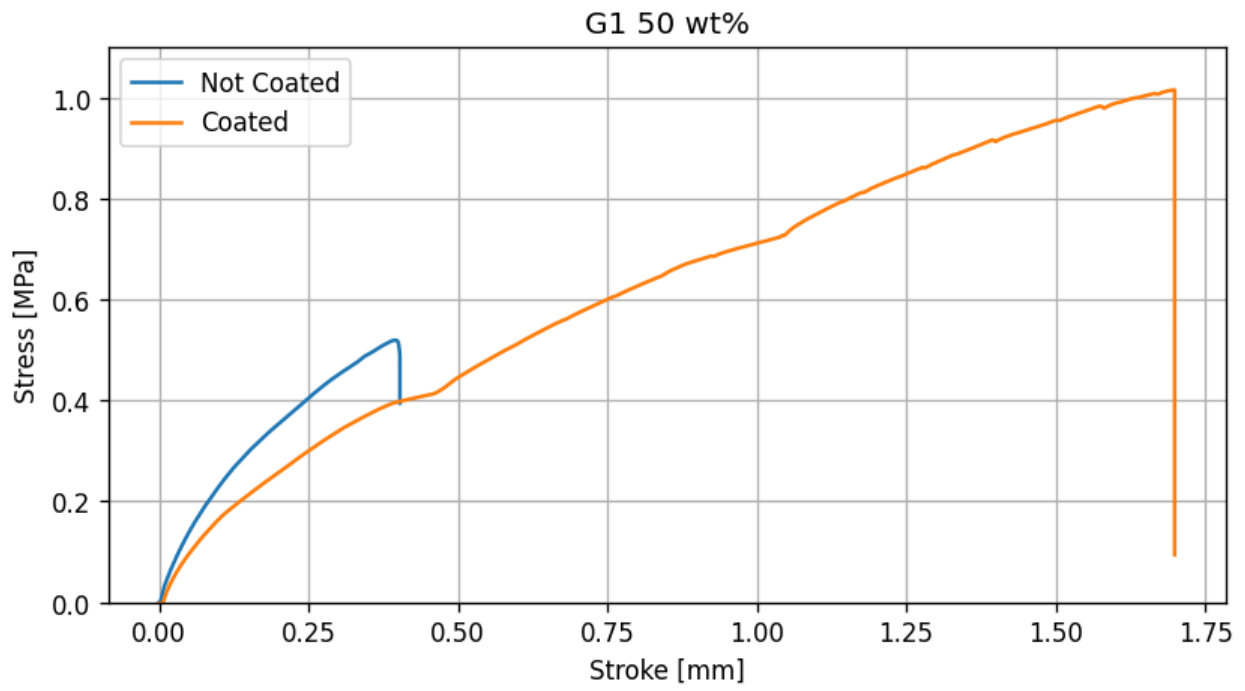
Figure B.5: Stress - strain curve of G1 50wt% uncoated and PAMA coated.
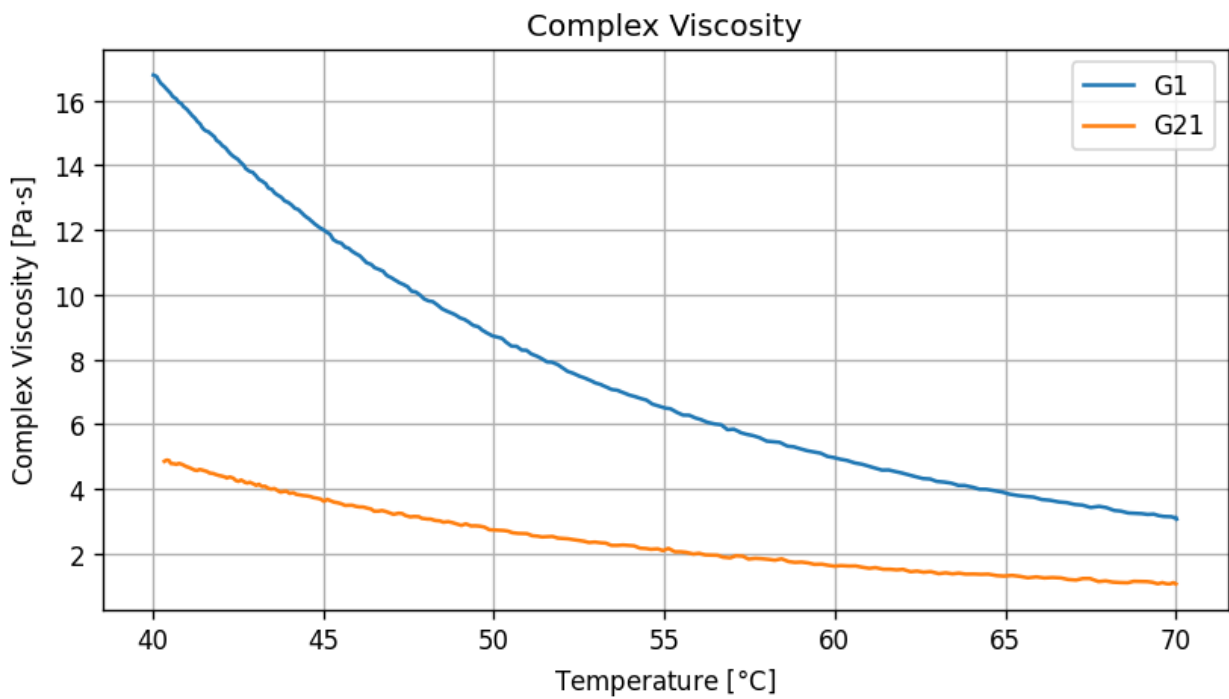
Figure B.6: Temperature sweep of G21 and G1 polysulphides.

C Appendices

The following theoretical calculation aims to understand the relationship between the stress-strain curves of G21 1:1 on PAMA coated glass, aluminium and polycarbonate surfaces, and how the bond energies play a role in the adhesive system.

Firstly, it is important to define the assumptions made during these calculations because it allows for the simplification of the complex real-life calculation and helps to set up a baseline with defined variables to work with.

Assumptions:

1. The failure mode of all three samples was adhesion failure, and the total energy (adhesion energy) was solely involved in breaking the C-S bonds between the PAMA coating on the surface and the polysulphide-TTT network.

2. The compositions of the different surfaces were not taken into account—in other words, the surface energies and other parameters related to surfaces.

3. The energy required to break 1 mol of C-S bonds is 259 kJ.[40]

4. Thickness of the PAMA coating was assumed to be 500 nm and constant for all surfaces.

5. The density (ρ) of PAMA coating was assumed to be 1 g/cm^3

6. All the allyl groups are assumed to be on the surface of the PAMA coating.

7. The PAMA coating is solely composed of AMA molecules.

Example calculation for G21 1:1 on PAMA coated glass surface:

The average adhesion energy for this sample was obtained to be 0.387 J, refer to *Table A.3*. This energy is involved in breaking the C-S bonds between the PAMA coated glass and the adhesive bulk, however, there are two PAMA coated surfaces that are in contact with the adhesive bulk. Hence, focusing on only one surface - bulk interaction results in an adhesion energy of 0.1935 J.

Since,

$$n(C - S) : Energy$$
$$1 \ mol : 259000 \ J$$
$$x \ mol : 0.1935 \ J$$

Therefore,

$$x = 7.47 \cdot 10^{-7} \ mol$$

For x is the number of moles of C-S bonds that were responsible for the adhesion forces.

Now to find out the contribution of the PAMA coating to this adhesion force, the total number of allyl groups on the glass surface needs to be calculated.

Since the thickness is assumed to be 500 nm and the area is known to be 312.5 mm^2, refer to *Figure 2.1*. It is possible to calculate the volume, which is $1.56 \cdot 10^{-4}$ cm^3.

The mass (m) of the PAMA coating can be calculated:

$$m = \rho \cdot V_{coating}$$
$$m = 1g/cm^3 \cdot 1.56 \cdot 10^{-4} cm^3$$
$$m = 1.56 \cdot 10^{-4} g$$

Because it is assumed that the PAMA coating is composed of AMA molecules only, the total moles of AMA can be calculated, since there is no change in the chemical structure apart from the joining of the AMA

molecules. Each AMA molecule contains one allyl group. Calculating the moles of AMA in the coating is equivalent to the moles of allyl groups. The molecular weight of AMA is 126.16 g/mol.

$$n = \frac{m}{Mr}$$

$$n = \frac{1.54 \cdot 10^{-4} \ g}{126.16 \ g/mol}$$

$$n = 1.24 \cdot 10^{-6} \ mol$$

Therefore, the total moles of allyl groups on the PAMA coating is $1.24 \cdot 10^{-6}$ mol. This is equivalent to the total possible C-S bonds between the PAMA coating and the bulk of the adhesive.

Thus, it is possible to calculate how efficient the coating. From the energy calculations, the actual moles of C-S bonds are obtained. And, the previous calculations obtained the total possible moles of C-S bonds that can occur.

Hence, the efficiency of the PAMA coating is:

$$\eta = \frac{actual \ C - S \ bonds}{total \ C - S \ bonds}$$

$$\eta = \frac{7.47 \cdot 10^{-7} \ mol}{1.24 \cdot 10^{-6} \ mol}$$

$$\eta = 0.602 = 60.2\%$$

Similarly, the above calculations were repeated for the aluminium and polycarbonate surfaces.

Table C.1: The effective contribution of the PAMA coating for the adhesive system of G21 1:1

Surface	η [%]
Glass	60.2
Aluminium	19.3
Polycarbonate	10.6

The table above represents the efficiency of the PAMA coating for the given surfaces with the G21 1:1 adhesive. The theoretical calculations agree with the experimental results for the difference between the glass and polycarbonate samples. As the efficiency reduces so does the adhesive strength, additionally, it further explains the temporary stress reductions in the stress-strain curves. For polycarbonate samples the PAMA coating efficiency is significantly lower than the glass samples. This reduction in efficiency suggests fewer SH groups were involved in the surface-bulk interface.

Hence, more C-S bonds in the adhesive bulk, thus, creating a dense rigid network leading to brittleness. This is demonstrated by the lap shear test, which reveals that the polycarbonate sample has lower adhesion strength and shows no indications of temporary stress reduction due to the brittle and rigid nature of the adhesive bulk.

However, the theoretical calculation does have limitations due to the assumptions made to simplify the calculation. This limitation is seen for the case of aluminium samples. The efficiency of the PAMA coating for aluminium is calculated to be 19.3%, this value is significantly lower than glass and similar to polycarbonate, thereby suggesting that aluminium should behave similar to polycarbonate, but it does not, it behaves similar to glass. Therefore, there are additional factors at play here that need to be explored thoroughly in the future.